Electrochimica Acta 256 (2017) 81–89

Contents lists available at ScienceDirect

Electrochimica Acta

journal homepage: www.elsevier.com/locate/electacta

Research Paper

State of health estimation of battery modules via differential voltage analysis with local data symmetry method

Limei Wang*, Xiuliang Zhao, Liang Liu, Chaofeng Pan

Automotive Engineering Research Institute, JiangSu University, Zhenjiang 212013, China

ARTICLE INFO

Article history:
Received 14 July 2017
Received in revised form 21 September 2017
Accepted 3 October 2017
Available online 5 October 2017

Keywords:
State of health
Differential voltage analysis
Local data symmetry method
Lithium battery module
Electric vehicle

ABSTRACT

Cyclic voltammogram (CV) and differential voltage analysis (DVA) are two effective techniques to analyze the aging mechanism and estimate the aging state of a battery. However, the effectiveness of the two methods reported previously is based on single battery cells. In this paper, a comparison of the two methods is stated, and the equivalent relation is further derived. Besides, a local data symmetry method is introduced to calculate the differential voltage (DV) curve. The DV curves calculated by the proposed method are much smoother than that by the numerical-derivative method. Based on the location interval of two inflection points in the DV curve, a new method is inferred for lithium iron phosphate ($LiFePO_4$) battery cells, and is applied to estimate the state of health (SOH) of battery modules. The applicability of the method is further verified via battery module simulation and experimental data. The results show that the DV curves fluctuate and do not overlap in the voltage plateau region due to the uneven currents flowing through each in-parallel battery cells. There is also a good linear regression of the two inflection point location interval versus battery module capacity within 2% error bounds, suggesting that the DVA method inferred from battery cells can be directly applied to battery modules.

1. Introduction

The growing concern over energy and environmental crisis has greatly stimulated the research and development of electric vehicles (EVs) [1,2]. Lithium-ion batteries (LIBs), as an essential part of EVs, have been intensively preferred because of their high energy density and safety [3,4]. However, the short cycle life of LIBs remains tremendous challenge to the further commercialization of EVs. The battery cycle life continuously deteriorates due to irreversible physical and chemical reactions [5]. A great insight to battery chemical reactions and aging mechanisms is conducive to design optimal battery management strategy [6]. The cyclic voltammogram (CV) has become a popular approach to analyze aging mechanisms within the battery. The locations of the CV peaks are related to battery aging state [7]. But the CV is generally measured by electrochemical workstation, which seems to be unsuitable for on-board implementation with in-situ operational data.

To describe the aging state of a battery, the state of health (SOH) is promulgated by the battery management system (BMS) [8–10]. SOH is a 'measure' that reflects the current state, including capacity and impedance, in relative to the original state of the battery [11]. A series of model-data fusion approaches are proposed for on-line SOH evaluating. Generally, these are the Recursive Least Square (RLS) method [12], Extended Kalman Filtering (EKF) method [13], Multivariate Adaptive Regression Splines (MARS) method [14], Support Vector Machine (SVM) method [15] and Particle Filter (PF) method [16]. However, the above mentioned methods are highly dependent on the adopted battery model and the accuracy of the model's parameters [1].

In recent years, incremental capacity analysis (ICA) and differential voltage analysis (DVA) are available to estimate the aging state and SOH of a battery [17–26]. The two methods originate from the study of intercalation process of battery materials [6]. ICA can be achieved by differentiating charged or discharged capacity (dQ/dV) with respect to terminal voltage (V). The aging mechanisms are then described by the peak amplitude and position of the dQ/dV–V (IC) curve [17–19]. Moreover, the adaptability of the ICA to analyze aging mechanisms of different LIBs from different manufactures is reported previously [20]. Correspondingly, DVA studies the aging state by using the relation of charged or discharged capacity (Q) to differential voltage (dV/dQ). As for ICA, many researchers have studied how the DV curve changes during battery cycle life [21–24]. Furthermore, the

* Corresponding author.
E-mail addresses: wanglimei@ujs.edu.cn, wanglimeisdh@sina.com (L. Wang).

https://doi.org/10.1016/j.electacta.2017.10.025
0013-4686/

Table 1
Specifications of equipment and parameters of battery cells.

Item	Model	Manufacturer	Characteristics
Temperature and humidity test chamber	BE-TH-225L8	Dongguan Bell Experiment Equipment Co., Ltd.	Temperature: −70 ~ 150 °C (±1 °C); Humidity: 20 ~ 98%
Battery performance tester	NBT5V10A	NingBo BaTe Technology Co., Ltd.	Voltage: 0 ~ 5 V (0.05% FS); Current: 150 mA ~ 10 A (0.05% FS)
Battery performance tester	NBT5V100A	NingBo BaTe Technology Co., Ltd.	Voltage: 0 ~ 5 V (0.05% FS); Current: 300 mA ~ 100 A (0.05% FS)
$LiFePO_4$ battery	JL-8Ah	Jiuli Energy Co., Ltd	Rated capacity: 8 Ah; Rated voltage: 3.2 V

possibility of the two methods has been validated for on-line SOH estimation [25,26]. And a battery SOH monitoring framework is also inferred to realize effective on-line SOH estimation.

Since the measured voltage contains noise, it is inevitable that the disturbance is brought into the calculated IC or DV curve [25,26]. There is difficulty in identifying the peaks lying within the plateau region of *V*-*Q* curve, where the peaks are submerged by the measurement noise. A solution is to use a fifth order polynomial to fit the measured *Q*-*V* curve. The IC curve is then calculated from the fitted curve [25]. Similarly, a second order polynomial is used to smooth the DV curve calculated from the numerical-derivative method [26]. The results of the polynomial fitting method are constrained by the selected data range and the order of the polynomial. Although high-degree polynomial order achieves higher fitting precision, a higher computing time is the greatest cost. Currently, the support vector regression method is also introduced to calculate the IC curve [25]. However the computational efficiency of the method is also low, as it involves a matrix element. Therefore, a higher efficiency method is needed for obtaining the IC or DV curve.

In applications, a battery module generally consists of several small battery cells connected in parallel to meet the capacity requirement. The battery modules are then assembled in series to achieve the required voltage in EVs [27,28]. If there is no difference among the in-parallel battery cells, a battery module could be regarded as a single large capacity battery. Unfortunately, due to the inconsistent manufacturing processes and operating environments, battery cell variations cannot be eliminated [1,29]. The inconsistency among in-parallel battery cells will lead to uneven current flowing through each battery cell branch even if the battery module is charged or discharged using a constant current [30]. In addition, the current of in-parallel battery cell cannot be directly measured. Therefore, the applicability of ICA or DVA methods for SOH estimation of a battery module should be explicitly researched.

In this paper, the CV and DVA method is initially compared. Then the local data symmetry method is introduced to calculate the DV curve. Subsequently, a new method is proposed to estimate the SOH of battery modules based on the two inflection points in the DV curve. Finally, the applicability of the proposed method is validated by battery modules with different capacities, which are assembled by four lithium iron phosphate ($LiFePO_4$) battery cells in parallel.

2. Comparison of IC/DV and CV curve

A fixed voltage sweep rate is set to measure a battery within a certain limited voltage range. The relation between the reaction current and the sweep voltage is called CV, which can be described as [5]:

$$I = f_{CV}(V) \tag{1}$$

Where, I is the reaction current, and V represents the sweep voltage.

A fundamental function of a BMS is to monitor battery voltage, current and temperature [31]. Assuming the current following through a battery is constant, the (dis)charged capacity Q can be expressed as:

$$Q = It \tag{2}$$

Where, t is (dis)charge time.

Then the relation of (dis)charged capacity and voltage can be demonstrated as:

$$V = f(Q),\ Q = f^{-1}(V) \tag{3}$$

According to the principle of the ICA method, the IC curve can be described by Eq. (4).

$$(f^{-1})' = \frac{dQ}{dV} = \frac{d(It)}{dV} = \frac{Id(t)}{dV} = \frac{I}{dV/d(t)} = g(V) \tag{4}$$

Then the battery current can be deduced from Eq. (4):

$$I = \frac{dV}{dt} \cdot g(V) = f_{IC}(V) \tag{5}$$

Comparing Eq. (1) and Eq. (5), the two formulas are of the same form and type. The CV curve is subjected to the sweep voltage and reaction current. And the IC curve is dependent on the current and differential voltage dV/dt. In addition, the sweep rate of voltage in the CV is constant, whereas the dV/dt in the ICA method is varying with time. The ICA or DVA method presents the similar qualitative results as the CV based on the same mathematical derivation [6].

3. Cycle test and data analysis for battery cells

3.1. Testing system and schedule

Four $LiFePO_4$ battery cells with different aging states from a same manufacturer are randomly selected. For description purposes, the four battery cells are named from No. 1 to No. 4 battery cell, respectively. Table 1 lists the specifications of equipment and parameters of the battery cells. The four battery cells are performed cycle life test under the environmental temperature (25 °C), as described in Table 2. The battery cell voltage, current and (dis)charged capacity data are sampled synchronously with the sampling frequency of 1 Hz.

Table 2
Battery cycle test profile.

Step number	Step name		Stop condition
1	Rest	Duration: 30 min	
2	Charge	Current: 1C	Voltage >=3.65 V
3	Charge	Voltage: 3.65 V	Current <=1/10C
4	Rest	Duration: 30 min	
5	Discharge	Current: 1C	Voltage <= 2 V
6	Rest	Duration: 30 min	
7	Cycle	Step 2 to 6	

3.2. Charge voltage curve analysis

The battery discharge current is subjected to the driving condition of EVs, and the discharge current changes drastically during driving condition. The charge *V*-*Q* curve is specially illustrated as the charge current is constant under most conditions for EVs. Fig. 1 shows charge *V*-*Q* curves under different cycle numbers of No. 1 battery cell. It can be seen from the figure that the constant voltage charging phase 'leads' with the increase of cycle number due to the decrease of battery capacity [32].

The charge *V*-*Q* curve can be described as $U_i = f(Q_i)$, $Q_i = Q_0 + i \cdot \Delta Q$, $i = 0, 1, 2, \ldots$ The numerical-derivative method is applied to acquire the IC or DV curve, which can be represented as:

$$\frac{dU_i}{dQ_i} = \frac{f(Q_{i+1}) - f(Q_i)}{\Delta Q} \tag{6}$$

Where, Q_0 is the remaining or initial battery capacity.

Fig. 2 gives the IC and DV curves of No. 1 battery cell according to Eq. (6). Although the results do yield a clear change on the peaks of the curves, there is much disturbance in the curves which are unsuitable for peak point identification computationally. A more robust method is needed for obtaining the IC and the DV curve.

3.3. IC and DV curve acquisition by local data symmetry method

Assuming that the charge *V*-*Q* data in a small data range (n data points) can be polynomial fitted by $y = a_0 + a_1 x$, the problem of calculating the IC and DV curve is transformed to solve the parameter a_1 according to Eq. (6). The calculated process is given in Fig. 3.

After defining a deviation function $T = \sum_{k=1}^{n} (y_k - a_0 - a_1 x_k)^2$, the parameter a_1 is then identified as follows: selecting an appropriate data range (n data points), the variables in the deviation function can be solved by the constraint $T(a_0^*, a_1^*) = \min T(a_0, a_1)$. By solving $\frac{\partial T}{\partial a_0} = 0$, $\frac{\partial T}{\partial a_1} = 0$, the constraint can be reformulated as:

$$\begin{bmatrix} n & \sum_{k=1}^{n} x_k \\ \sum_{k=1}^{n} x_k & \sum_{k=1}^{n} x_k^2 \end{bmatrix} \begin{bmatrix} a_0 \\ a_1 \end{bmatrix} = \begin{bmatrix} \sum_{k=1}^{n} y_k \\ \sum_{k=1}^{n} x_k y_k \end{bmatrix} \tag{7}$$

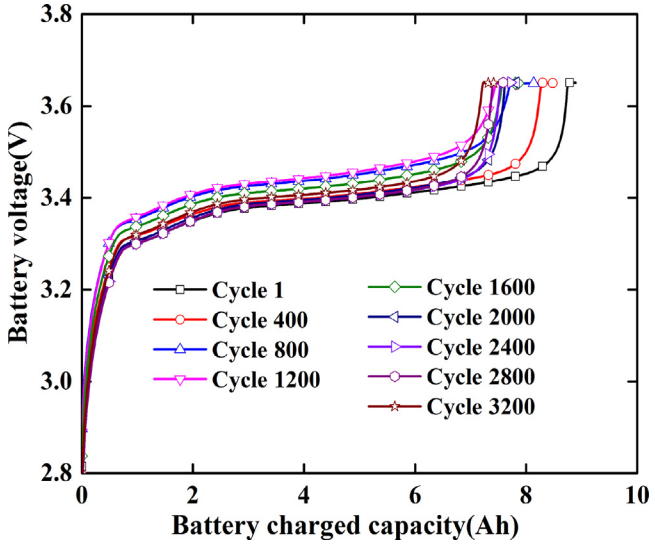

Fig. 1. Voltage-to-charged capacity curves with charge current of 1C.

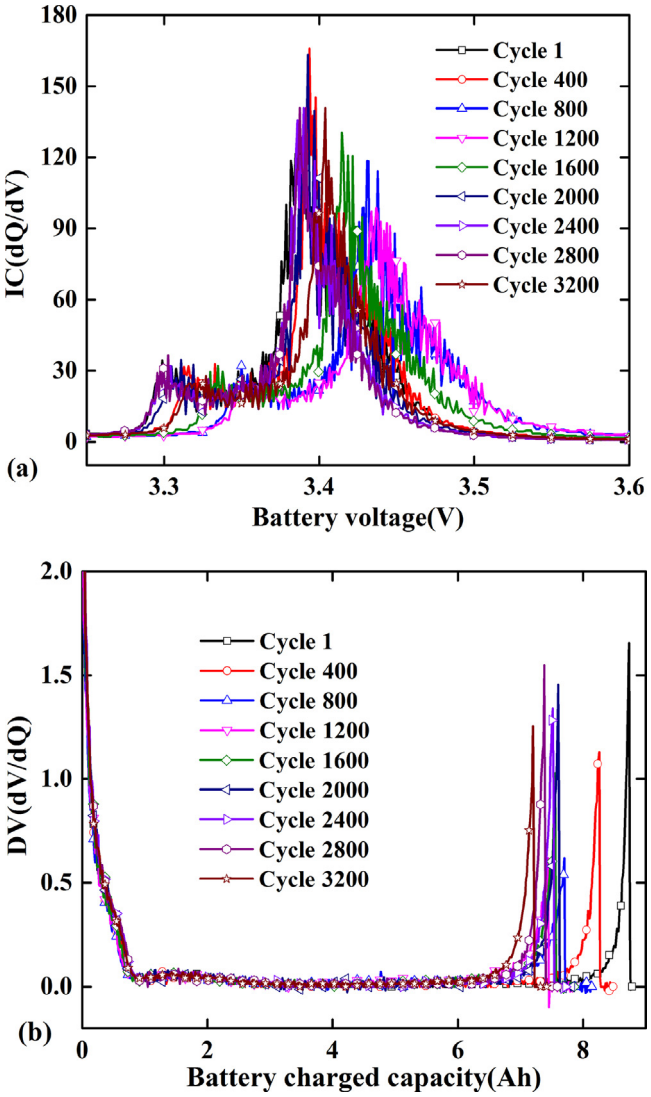

Fig. 2. (a) IC and (b) DV curve calculated by numerical-derivative method.

The coordinates of n data points can be expressed as $(-\frac{n}{2}, y_0), (-\frac{n}{2}+1, y_1), \ldots, (0, y_{\frac{n}{2}}), \ldots, (\frac{n}{2}, y_n)$, as shown in Fig. 3. The parameter a_1 can be solved by Eq. (7), which can be expressed as:

$$a_1 = \frac{\sum_{k=0}^{n} (-\frac{n}{2} + k) y_k}{\sum_{k=0}^{n} (-\frac{n}{2} + k)^2} \tag{8}$$

Fig. 4 shows the IC and DV curves of No. 1 battery cell with n being 20 by the local data symmetry method. The figure delivers the corresponding results calculated by the numerical-derivative method. It is obvious that the IC and DV curves are much smoother by using the local data symmetry method and the calculated efficiency is available for application. It can also be seen that the peak position and width obtained by the two methods are the same. The peak intensity is different due to the measured voltage noise. It is important to note that the variation trends of the peak intensity to the cycle number remain the same.

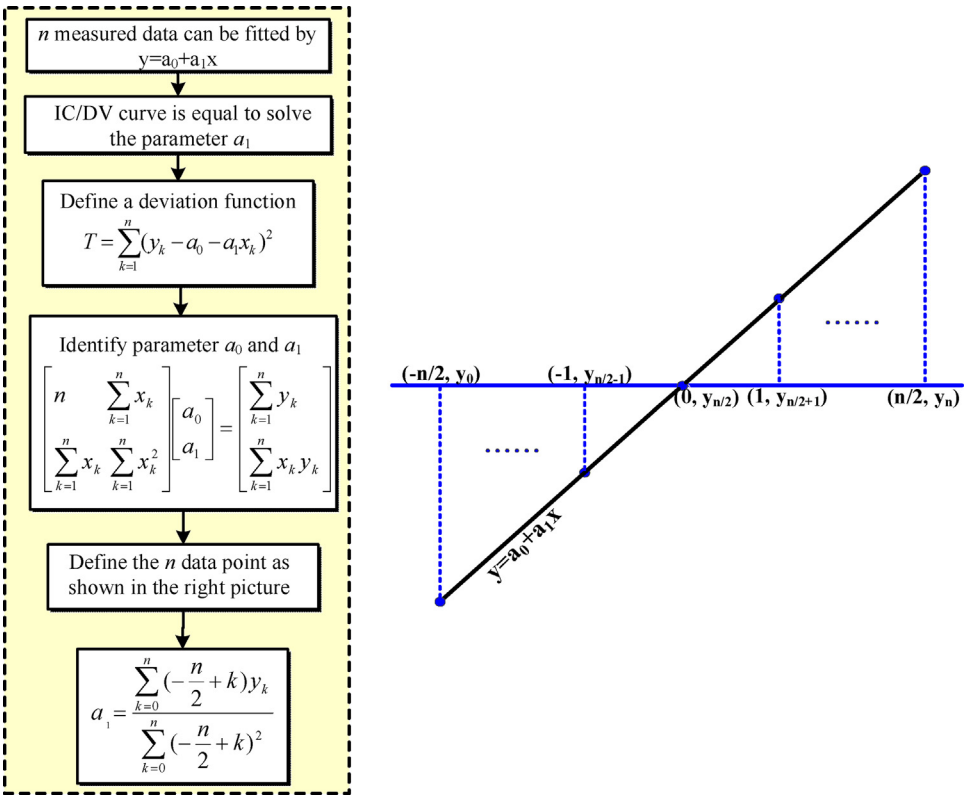

Fig. 3. Calculated process of local data symmetry method.

3.4. SOH estimation via differential voltage curve

The peaks of IC and DV curve are associated with the lithium-ion intercalation process, which can be used to analyze the aging state of a battery [6,32]. Comparing Fig. 4(a) with Fig. 4(b), the inflection points in the DV curve are observed to have good correlation with the cycle numbers for the tested battery cells. The ICA is subjected to the applied (dis)charge current. If ICA is applied to a charge voltage curve obtained under a high current rate, the reliability of detecting the peaks of the IC curve would be limited [6]. Fig. 5 shows the DV curves under different cycle numbers of the four tested battery cells. It is observed that the first inflection points (charged capacity being about 0.95 Ah) in the DV curves are almost overlapped, which suggests that the location of the first inflection point is non-sensitive to different battery cells. It is notable that the second inflection point moves 'forward' with the increase of cycle number. Therefore, the location of the second inflection point can be used to evaluate the battery cell SOH.

Taking the original capacity and the second inflection point location of No. 1 battery cell as benchmarks, Fig. 6 shows the relation between the normalized battery capacity and the normalized second inflection point location of the tested four battery cells. The solid line gives the fitted linear relationship between the two values while the dotted line gives the error bound of ±3.5%. There is a good relationship between the location of the second inflection point and battery capacity. The deviations between the points and the fitted linear curve are within 3.5%. Furthermore, it can also be discovered from the virtual elliptical area that there is an approximate fixed deviation between some points and the fitted linear curve.

For an EV, the charge current I is constant. According to the data standard current integration method, the charged capacity C can be written as:

$$C = C_0 + \sum It \tag{9}$$

Where, C_0 is the remaining or initial (dis)charged capacity, t is the sampling time.

To accurately calculate the charged capacity, a reasonable simplified assumption is defined that the battery starts charging from zero initial (dis)charged capacity, $C_0 = 0$. The fixed deviation shown in the virtual elliptical area may be caused by the initial errors shown in Eq. (9). As the first inflection point location is non-sensitive to the battery cells and the cycle numbers, this point can be addressed to eliminate the (dis)charged capacity initial error. Fig. 7 shows the correlation between the normalized two inflection points location interval and battery capacity. The figure indicates that there is good linear regression between them. The deviation between the points and the fitted linear curve is reduced to within 2.5% except for a few outliers, which verifies that the fixed deviation is caused by the initial error.

4. Cycle test and data analysis for battery modules

4.1. Simulation model established

In reality, it is inconvenient to select battery cells with an expected aging status for experiment. Simulation analysis is an effective and useful tool for exploring the battery cell inconsistency on the battery module DV curve.

In our previous report, the first RC block equivalent circuit model is adequate to describe the dynamic and the steady state characteristics of a battery cell [2]. The elements including the open circuit voltage E_m, the ohmic internal resistance R_0, the polarization resistance R_1 and capacitance C_1 in the first RC block equivalent circuit model are firstly built within the Simscape

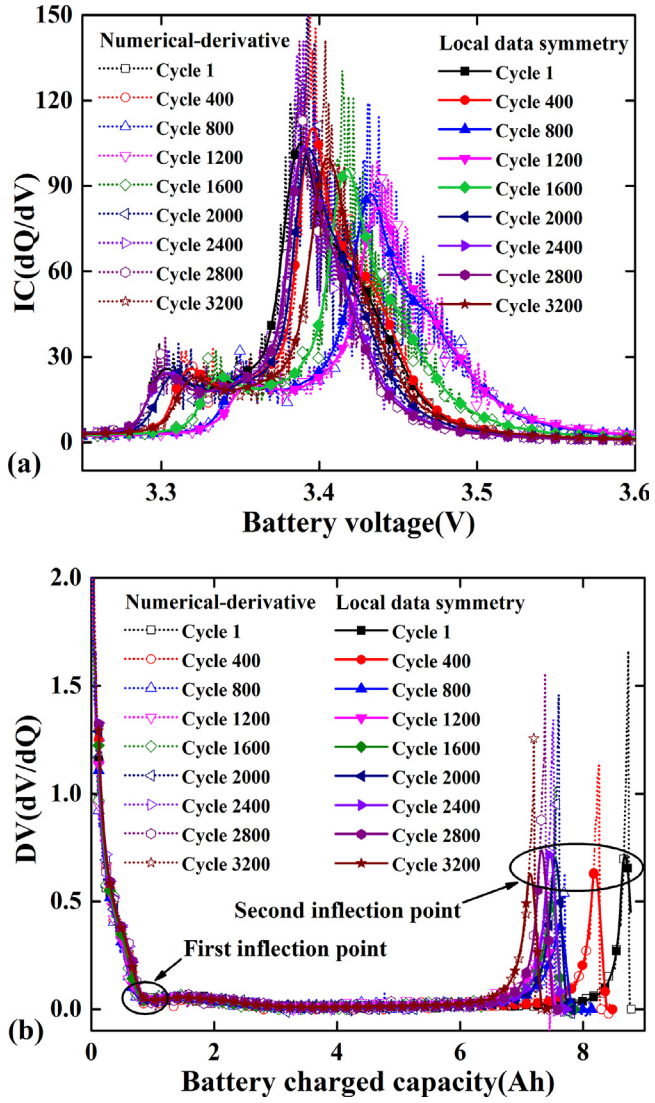

Fig. 4. (a) IC and (b) DV curve calculated by numerical-derivative and local data symmetry method.

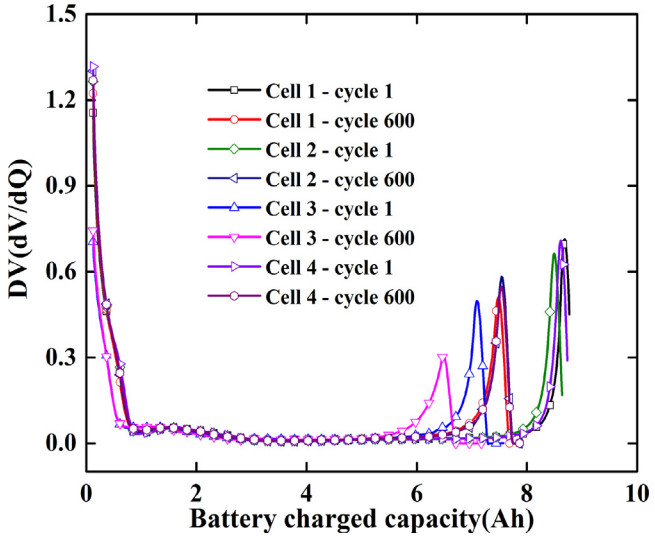

Fig. 5. DV curves for different battery cells.

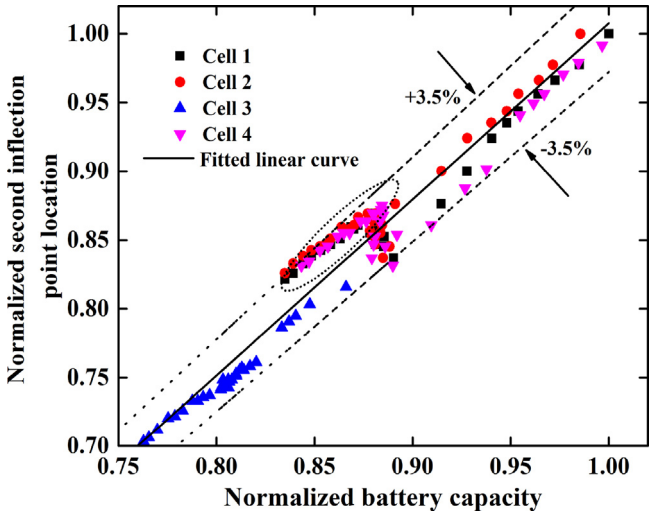

Fig. 6. Correlation between normalized second inflection point location and capacity.

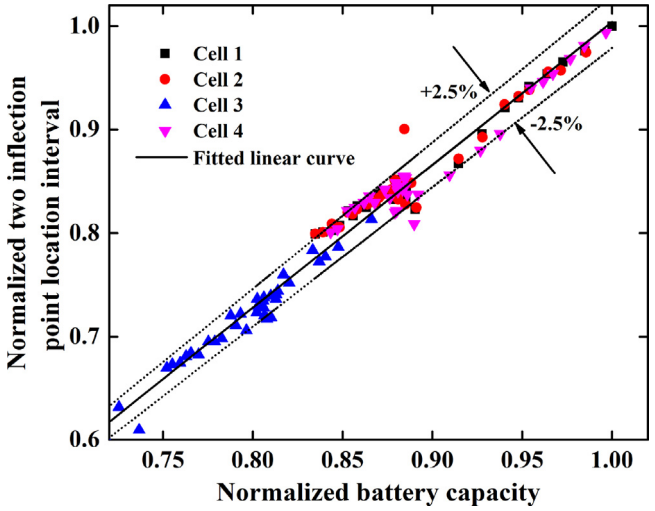

Fig. 7. Correlation between normalized two inflection point location interval and capacity.

language. The built elements are then assembled together to form a battery module model, as shown in Fig. 8. The specific modeling process and validation of the battery module model are referred in Ref. [2]. The simulation results agree well with the experimental data, and the maximum error is to within 1%. According to the 'battery cycle test profile' shown in Table 2, the four battery cells are cycle life tested. The relation between the capacity and ohmic internal resistance under different cycle numbers are extracted and shown in Fig. 9. Seen from the figure, there is a constraint between them, which can be described as:

$$\frac{R_0}{R_{0,org}} = 24.29\left(\frac{C}{C_{org}}\right)^2 - 47.62\left(\frac{C}{C_{org}}\right) + 24.32 \quad (10)$$

Where, $R_{0,org}$ is the initial ohmic internal resistance and C_{org} represents the initial battery capacity. The constraint described in Eq. (10) provides a basis for setting the aging state of the in-parallel battery cells.

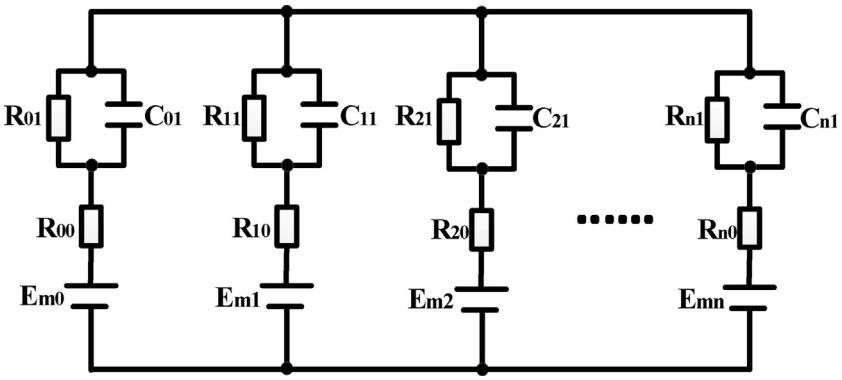

Fig. 8. Schematic of battery module.

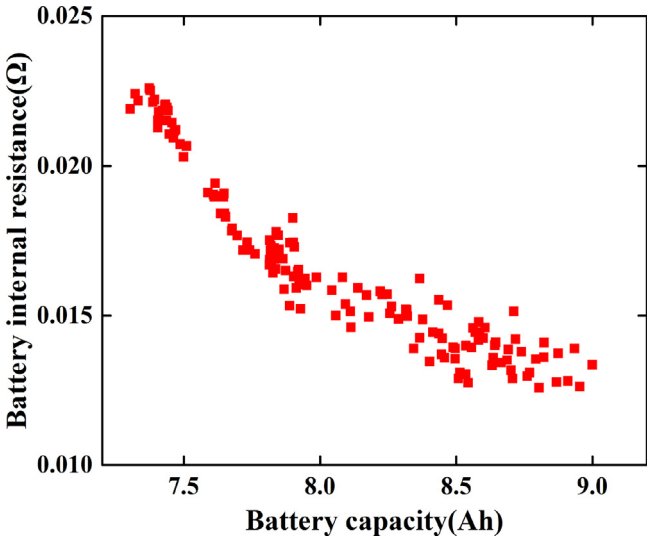

Fig. 9. Constraint between capacity and internal resistance for tested battery cells.

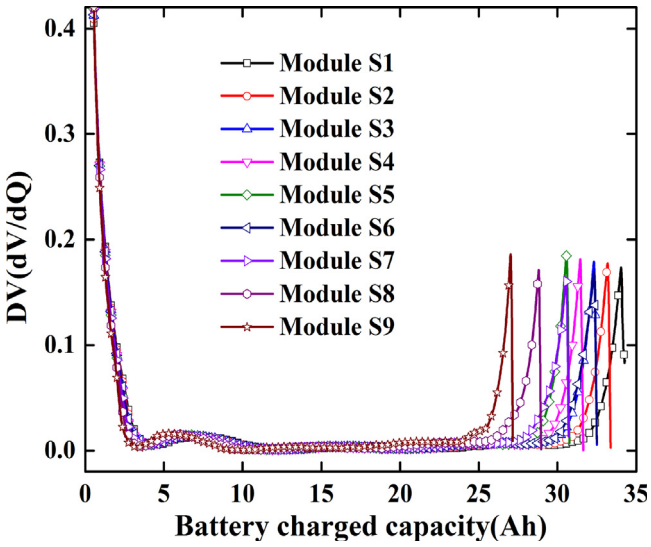

Fig. 10. DV curves of the simulated battery modules shown in Table 3.

4.2. Simulated results analysis

Battery module with inconsistent battery cells (capacity and resistance) is simulated using the battery module model described in Section 4.1. The parameters of nine simulated battery modules with four in-parallel battery cells, as shown in Fig. 8, are listed in Table 3. The capacity decrease coefficients for each battery cell are also listed in Table 3. "x" represents that the current capacity is x times of the initial battery capacity. Meanwhile, the corresponding internal resistance increase coefficient is calculated from the constraint expressed in Eq. (10).

The DV curves of the nine simulated battery modules are shown in Fig. 10. And the correlation between the two inflection points location interval and capacity of the nine battery modules are shown in Fig. 11. Fig. 11 also provides the relation between the first inflection point location and battery capacity. It can be seen from the two figures that the first inflection point location also changes linearly with the battery capacity, and the slope is about 0.125.

Table 3
Parameters of simulated battery modules with four in-parallel battery cells.

Battery module	Total capacity (Ah)	Individual capacity decrease coefficient
Module S1	34.40	1, 1, 1, 1
Module S2	33.90	0.9, 1, 1, 1
Module S3	33.15	0.9, 0.9, 1, 1
Module S4	32.33	0.9, 0.9, 0.9, 1
Module S5	31.48	0.9, 0.9, 0.9, 0.9
Module S6	33.18	0.8, 1, 1, 1
Module S7	31.48	0.8, 0.8, 1, 1
Module S8	29.75	0.8, 0.8, 0.8, 1
Module S9	28.00	0.8, 0.8, 0.8, 0.8

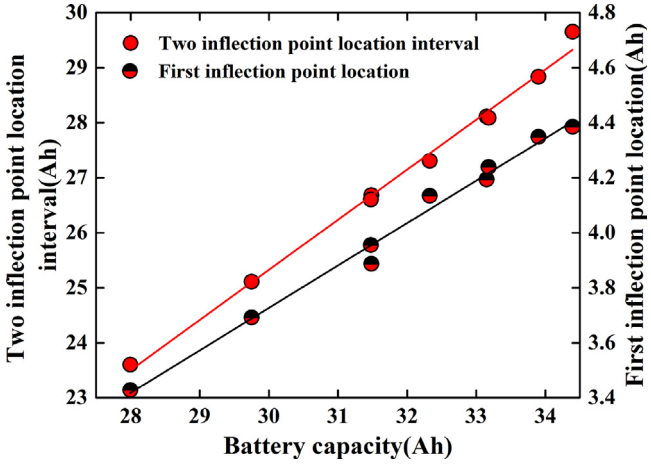

Fig. 11. Correlation between two inflection point location interval and capacity of the simulated battery modules shown in Table 3.

Table 4
Parameters of simulated battery modules with different in-parallel battery cells.

Battery module	Total capacity (Ah)	Numbers of in-parallel battery cells	Individual capacity decrease coefficient
Module P1	33.90	4	0.9, 1, 1, 1
Module P2	32.31	4	0.8, 0.9, 1, 1
Module P3	42.69	5	0.9, 1, 1, 1, 1
Module P4	41.04	5	0.8, 0.9, 1, 1, 1
Module P5	51.47	6	0.9, 1, 1, 1, 1, 1
Module P6	49.69	6	0.8, 0.9, 1, 1, 1, 1
Module P7	60.13	7	0.9, 1, 1, 1, 1, 1, 1
Module P8	58.45	7	0.8, 0.9, 1, 1, 1, 1, 1
Module P9	68.78	8	0.9, 1, 1, 1, 1, 1, 1, 1
Module P10	67.07	8	0.8, 0.9, 1, 1, 1, 1, 1, 1

When a battery capacity decays to 80% of its original value, it cannot be served as a power battery [33]. For the tested battery cell, the rated capacity is about 8 Ah. The maximum battery capacity inconsistency is about 1.6 Ah. The first inflection point location moves about 0.2 Ah, which coincides with the results in Section 3.4 and can be neglected in practical application.

For a battery module, the first inflection point is unsuitable for calibrating the battery charged capacity individually as the change is more obvious. Considering the initial error of the battery module, the location interval of the two inflection points is more suitable for battery module SOH estimation. As can be seen from Fig. 11, there is also a good linear regression between them, suggesting that the proposed DVA method inferred from the battery cell can be directly applied to battery modules.

Another set of simulated battery modules with different numbers of in-parallel battery cells are also established and examined to validate the applicability of proposed DVA method. The specific parameters of these battery modules are listed in Table 4. The corresponding results are shown in Figs. 12 and 13. The good linear relationship among them further confirms that the two inflection points location interval is more suitable for battery module SOH estimation and the proposed DVA method can be directly applied to battery modules.

4.3. Test results analysis

Four $LiFePO_4$ battery cells are assembled as a battery module to conduct the cycle life testing. The parameters of the chosen battery cells are listed in Table 1. Before cycle life testing, the capacity of each battery cell is measured according to the '2010 EV lithium-ion power battery test specification'. The original capacity of each battery cell is 8.83 Ah, 8.80 Ah, 8.85 Ah, 8.76 Ah. Subsequently, the four battery cells are connected in-parallel for cycle life testing. The battery module and cell voltage, current and (dis)charged capacity data are sampled synchronously with sampling frequency of 1 Hz.

Fig. 14 shows the cycle DV curves of the tested battery module. Compared with the battery cells, the battery module DV curves fluctuate and do not overlap in the voltage plateau region within the plateau region of the *V*-*Q* curve. The in-parallel battery cell

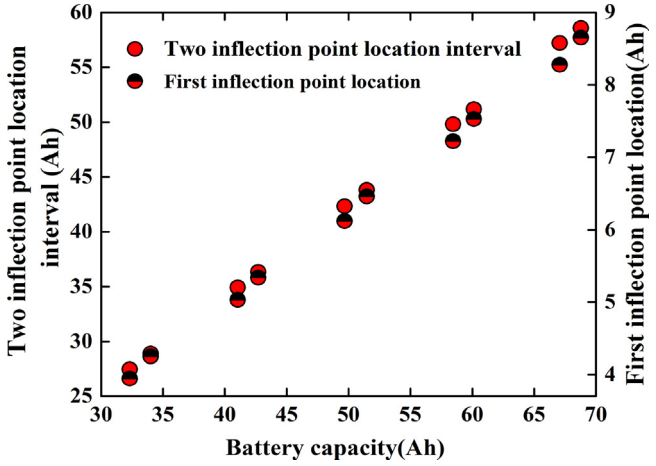

Fig. 13. Correlation between two inflection point location interval and capacity of the simulated battery modules shown in Table 4.

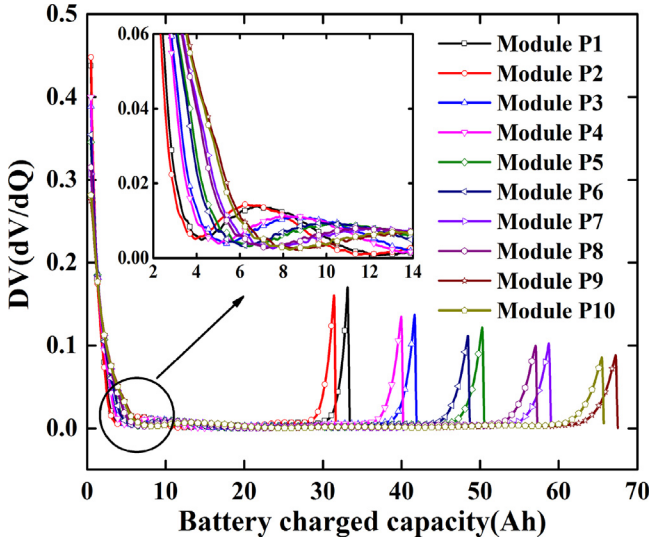

Fig. 12. DV curves of the simulated battery modules shown in Table 4.

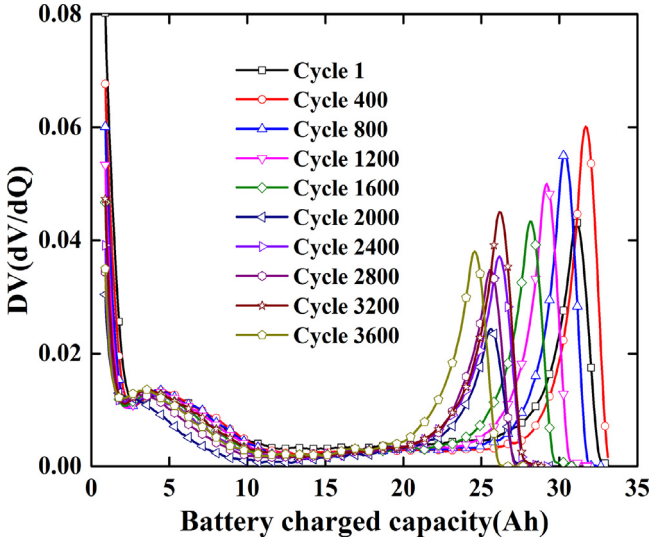

Fig. 14. DV curves of tested battery module.

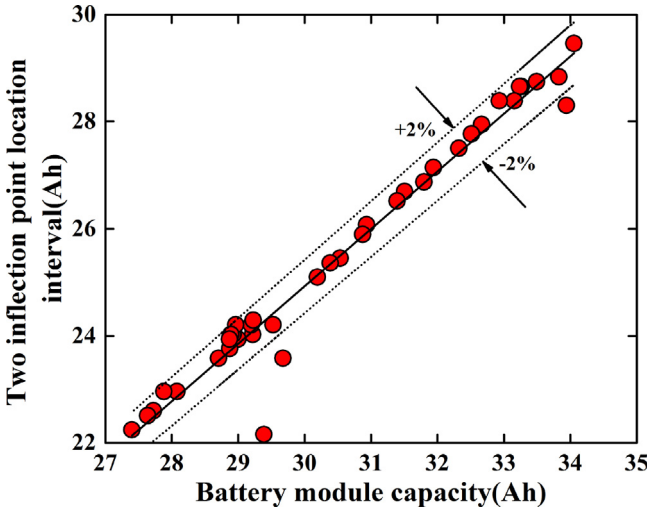

Fig. 15. Correlation between two inflection point location interval and capacity of tested battery module.

inconsistency leads to uneven and fluctuant currents flowing through each battery cell branch even if the battery module is charged using a constant current. The DV curves are also influenced by the fluctuant currents. Fig. 15 presents the correlation between the location interval of the two inflection points and capacity of the tested battery module. The figure indicates that there is a good linear regression between the two inflection points location interval and battery capacity. The deviation among the points and the fitted linear curve is within 2% except for a few outliers. Therefore, the location interval of the two inflection points very strongly indicates a robust aging signature for a $LiFePO_4$ battery module, as demonstrated by simulation and experimental results.

For the battery module from the same manufacturer, the relationship between the location interval of the two inflection points and battery capacity should be established off-line. In application, the measured *V*-*Q* curve is performed by the local data symmetry method to acquire the corresponding DV curve. The battery module SOH is then estimated by the off-line calibrated relationship when the calculated DV curve reaches the second inflection point.

5. Conclusions

In this work, a comparison of CV and DVA method is stated and the equivalent relation of CV and DVA method is further derived. A new method – local data symmetry method, is introduced to calculate the DV curve. Compared with the previous numerical-derivative method, the proposed local data symmetry method provides more robust and smoother DV curve.

Based on the location interval of two inflection points in the DV curves, a new method is proposed to estimate the SOH of the battery module, which is inferred from single $LiFePO_4$ battery cells. The applicability of proposed DVA method is further studied through battery module simulation and experimental data. The results show that the cycle DV curves fluctuate and do not overlap in the voltage plateau region due to the uneven current flowing through each in-parallel battery cell. There is also a good linear regression between the two inflection points location interval versus the battery module capacity within 2% error bounds. This suggests that the proposed DVA method inferred from battery cells can be directly applied to battery modules.

The sensitivity of the proposed method under different operating conditions will be further investigated, and the implementation of the method within an actual BMS will be tested.

Acknowledgements

This work is supported by the National Natural Science Foundation of China (51707084), the Natural Science Fund project in Jiangsu Province (BK20160529, BK20140563, BK20171300), the China Postdoctoral Science Foundation (2016M591775), the Research Funds for Senior Professionals of Jiangsu University (15JDG165), the National Key Technology R&D Program of China (2015BAG07B00) and the Special Funds for the Transformation of Scientific and Technological Achievements in Jiangsu Province (BA2016162).

References

[1] L.M. Wang, Y. Cheng, X.L. Zhao, A $LiFePO_4$ battery pack capacity estimation approach considering in-parallel cell safety in electric vehicles, Applied Energy 142 (2015) 293–302.
[2] L.M. Wang, X.L. Zhao, L. Liu, et al., Battery pack topology structure on state-of-charge estimation accuracy in electric vehicles, Electrochimica Acta 219 (2016) 711–720.
[3] A. Farmann, D.U. Sauer, A comprehensive review of on-board State-of-Available-Power prediction techniques for lithium-ion batteries in electric vehicles, Journal of Power Sources 329 (2016) 123–137.
[4] A. Farmann, W. Waag, D.U. Sauer, Adaptive approach for on-board impedance parameters and voltage estimation of lithium-ion batteries in electric vehicles, Journal of Power Sources 299 (2015) 176–188.
[5] Southampton electrochemistry group, Instrumental Methods in Electrochemistry, Ellis Horwood, London, 1985, pp. 178–227.
[6] A. Farmann, W. Waag, A. Marongiu, et al., Critical review of on-board capacity estimation techniques for lithium-ion batteries in electric and hybrid electric vehicles, Journal of Power Sources 281 (2015) 114–130.
[7] X.N. Feng, J.Q. Li, M.G. Ouyang, et al., Using probability density function to evaluate the state of health of lithium-ion batteries, Journal of Power Sources 232 (2013) 209–218.
[8] Y.J. Zheng, L.G. Lu, X.B. Han, et al., $LiFePO_4$ battery pack capacity estimation for electric vehicles based on charging cell voltage curve transformation, Journal of Power Sources 226 (2013) 33–41.
[9] J. Groot, State-of-health estimation of li-ion batteries: Cycle life test methods [dissertation], Chalmers University of Technology, Göteborg (Sweden), 2012.
[10] Y. Zou, X.S. Hu, H.M. Ma, et al., Combined state of charge and state of health estimation over lithium-ion battery cell cycle lifespan for electric vehicles, Journal of Power Sources 273 (2015) 793–803.
[11] C.H. Weng, X.N. Feng, J. Sun, et al., State-of-health monitoring of lithium-ion battery modules and packs via incremental capacity peak tracking, Applied Energy 180 (2016) 360–368.
[12] X.S. Hu, F.C. Sun, Y. Zou, et al., Online estimation of an electric vehicle lithium-ion battery using recursive least squares with forgetting, 2011 IEEE American Control Conference, O'Farrell Street, San Francisco, CA, USA, 2011, pp. 935–940 IEEE.
[13] G.L. Plett, Extended Kalman filtering for battery management systems of LiPB-based HEV battery packs: Part 3. State and parameter estimation, Journal of Power Sources 134 (2004) 277–292.
[14] J.C. Álvarez Antón, P.J. García Nieto, F.J. de Cos Juez, et al., Battery state-of-charge estimator using the MARS technique, IEEE Transactions on Power Electronics 28 (2013) 3798–3805.
[15] J.C. Álvarez Antón, P.J. García Nieto, F.J. de Cos Juez, et al., Battery state-of-charge estimator using the SVM technique, Applied Mathematical Modelling 37 (2013) 6244–6253.
[16] Y.J. Wang, C.B. Zhang, Z.H. Chen, A method for joint estimation of state-of-charge and available energy of $LiFePO_4$ batteries, Applied Energy 135 (2014) 81–87.
[17] M. Dubarry, V. Svoboda, R. Hwu, et al., Incremental capacity analysis and close-to-equilibrium OCV measurements to quantify capacity fade in commercial rechargeable lithium batteries, Electrochemical and Solid-State Letters 10 (2006) A454–A457.
[18] M. Safari, C. Delacourt, Simulation-based analysis of aging phenomena in a commercial graphite/$LiFePO_4$ cell, Journal of Electrochemical Society 158 (12) (2011) A1436–A1447.
[19] A.J. Smith, J.C. Burns, J.R. Dahn, High-precision differential capacity analysis of $LiMn_2O_4$/graphite cells, Electrochemical and Solid-State Letters 14 (2011) A39–A41.
[20] W. Shi, X.S. Hu, C. Jin, et al., Effects of imbalanced currents on large-format LiFePO4/graphite batteries system connected in parallel, Journal of Power Sources 313 (2016) 198–204.

[21] I. Bloom, A.N. Jansen, D.P. Abraham, et al., Differential voltage analyses of high-power, lithium-ion cells: 1. Technique and application, Journal of Power Sources 139 (2005) 295–303.
[22] K. Honkura, K. Takahashi, T. Horiba, Capacity-fading prediction of lithium-ion batteries based on discharge curves analysis, Journal of Power Sources 196 (2011) 10141–10147.
[23] I. Bloom, J.P. Christophersen, D.P. Abraham, et al., Differential voltage analyses of high-power lithium-ion cells: 3. Another anode phenomenon, Journal of Power Sources 157 (1) (2006) 537–542.
[24] H.M. Dahn, A.J. Smith, J.C. Burns, et al., User-friendly differential voltage analysis freeware for the analysis of degradation mechanisms in Li-ion batteries, Journal of Electrochemical Society 159 (9) (2012) A1405–A1409.
[25] C.H. Weng, Y.J. Cui, J. Sun, On-board state of health monitoring of lithium-ion batteries using incremental capacity analysis with support vector regression, Journal of Power Sources 235 (2013) 36–44.
[26] L.M. Wang, C.F. Pan, L. Liu, et al., On-board state of health estimation of $LiFePO_4$ battery pack through differential voltage analysis, Applied Energy 168 (2016) 465–472.
[27] G.J. Offer, V. Yufit, D.A. Howey, et al., Module design and fault diagnosis in electric vehicle batteries, Journal of Power Sources 206 (2012) 383–392.
[28] L.M. Wang, Y. Cheng, X.L. Zhao, Influence of connecting plate resistance upon $LiFePO_4$ battery performance, Applied Energy 147 (2015) 353–360.
[29] B. Kenney, K. Darcovich, D.D. MacNeil, et al., Modelling the impact of variations in electrode manufacturing on lithium-ion battery modules, Journal of Power Sources 213 (2012) 391–401.
[30] R. Gogoana, M.B. Pinson, M.Z. Bazant, et al., Internal resistance matching for parallel-connected lithium-ion cells and impacts on battery pack cycle life, Journal of Power Sources 252 (2014) 8–13.
[31] Battery Test Manual for Plug-in Hybrid Electric Vehicles, Idaho National Laboratory, 2008.
[32] R. Yazami, Ph. Touzain, A reversible grarhite-lithium negative electrode for electrochemical generators, Journal of Power Sources 9 (1983) 365–371.
[33] J. Hubbman, Battery reference book, Bitrode Corporation, Missouri, USA, 2001.